Available at www.sciencedirect.com

ScienceDirect

http://www.elsevier.com/locate/biombioe

Effects of physical properties on one-dimensional downward smoldering of char: Numerical analysis

Fang He[a,b,*], *Nico Zobel*[b], *Wenjian Zha*[a], *Frank Behrendt*[b]

[a]*Shandong University of Technology, Zibo, Shandong 255091, PR China*
[b]*Berlin University of Technology, Berlin 10623, Germany*

ARTICLE INFO

Article history:
Received 4 November 2007
Received in revised form
24 January 2009
Accepted 10 February 2009
Published online 23 May 2009

Keywords:
Effects
Physical properties
One-dimensional downward smoldering
Char
Numerical analysis

ABSTRACT

Smoldering combustion in a packed bed of carbonaceous material is a very complex process, where numerous physical and chemical parameters are involved. This study was conducted to examine the impact of several physical parameters on the behavior of natural downward smoldering. For that purpose, a one-dimensional homogeneous model has been developed. Due to the fact that drying, pyrolysis or oxidative degradation occurs significantly faster than carbon oxidation, only the latter phenomenon was taken into account. The model was evaluated by comparison of numerical simulation results with experimental observations. Sensitivity analysis calculations of different physical properties of the bed material with respect to smoldering time, smoldering front velocity and front temperature suggest that in future experiments special attention should be devoted to accurate determination of bed shrinkage, bulk carbon density, mean void size, oxygen diffusivity in fuel bed.

1. Introduction

Downward smoldering of char often occurs in nature or some applications of our lives [1–7]. Typical examples are self-ignition of piles of sawdust, agricultural residues or any kind of flammable solid fuels. Even sometimes the ignition of the process is from inside and the fuel is not char, it would quickly develop into downward smoldering of char. This is because reverse propagation from inside to above surface is ten times faster than forward (here downward) propagation and char is often left after the smoldering front passing by [4]. Characteristic of downward smoldering is that it is forward smoldering with the product gases flow upward, which is in the reverse direction of smoldering propagation.

Smoldering process is not only hazardous but also an economic risk. However this process can also be utilized for space heating in green houses or corral as it is done in north China. For a better understanding of natural smoldering, several experimental and theoretical studies have been conducted in the last decades. Ohlemiller et al. [4,8–10] published experimental observations, a most comprehensive description of the sub-processes occurring during natural and forced-flow smoldering, and set up a complex model which was not solved. Fernandez-Pello et al. [11–16] investigated smoldering in foam under microgravity for reasons of fire safety in spacecrafts. The group of Hajaligol et al. [17–19] focused their research work on the study of smoldering in a cigarette. Despite these and numerous other studies in the field of smoldering [20–27], to our knowledge, no systematic theoretical investigation on the effects of physical parameters on natural downward smoldering has been undertaken so far.

* *Corresponding author*. Shandong University of Technology, Zibo, Shandong 255091, PR China.
E-mail address: hf@sdut.edu.cn (F. He).
0961-9534/$ – see front matter © 2009 Published by Elsevier Ltd.
doi:10.1016/j.biombioe.2009.02.008

Nomenclature

A	pre-exponential factor of char oxidation (s^{-1})
A_{cc}	pre-exponential factor of the ratio of CO to CO_2 in char oxidation (s^{-1})
c	specific heat (J kg^{-1} K^{-1})
C_1	ratio of oxygen to carbon mass consumption rate during carbon oxidation
C_2	Stefan-correction factor for convective heat transfer coefficient
$[C_{O_2}]$	mole concentration of oxygen at reaction front (mol m^{-3})
D	diffusivity (m^2 s^{-1})
E	activation energy of char oxidation (J mol^{-1})
E_{cc}	activation energy of the ratio of CO to CO_2 in char oxidation (J mol^{-1})
Gr	Grashof number
ΔH^{ref}	standard reaction enthalpy (J kg^{-1})
J	index of the reaction cell
k	heat conductivity (W m^{-1} K^{-1})
L_0	thickness of the original fuel bed (m)
L_c	character size (width of fuel bed) in surface heat convection calculation (m)
L_i	initial thickness of the ash layer (m)
L_h	initial thickness of the heated char layer (m)
L_f	distance between smoldering front and top surface (m)
L_w	thickness of insulation material (m)
M	molecular weight (kg $kmol^{-1}$)
$\dot{m}$	mass flux density (kg m^{-2} s^{-1})
n	selectivity of CO during oxidation
N	total number of finite volume cells for fuel bed
N1	total number of finite volume cells for insulation materials
Nu	Nusselt number
p	pressure (Pa)
Pr	Prandtl number
$\dot{q}$	heat flux density (W m^{-2})
$\dot{r}_C$	carbon oxidation rate (kg m^{-2} s^{-1})
R	universal gas constant (J mol^{-1} K^{-1})
sh	shrinkage of bed (ratio of bulk ash size to bulk char size)
t	time (s)
Δx	length of finite volume cell (m)
T	temperature (K)
T_i	ignition temperature (K)
V	velocity of smoldering front (m s^{-1})
w	mass fraction

Greek symbols

α	convective heat transfer coefficient (W m^{-2} K^{-1})
χ	average void size in porous bed (m)
ε	emissivity
σ	Stefan–Boltzmann constant (W m^{-2} K^{-4})
ρ	density (kg m^{-3})
Φ	void fraction in the packed bed

Subscript and superscript

a	pertinent to ash (as a solid)
a-char	pertinent to ash in the char bed
ash	pertinent to ash bed (bulk value)
b	bottom of fuel bed
C	pertinent to carbon
c-char	pertinent to carbon in the char bed
char	pertinent to char
CO	pertinent to carbon monoxide
CO_2	pertinent to carbon dioxide
eff	effective value
f	pertinent to smoldering front
g	pertinent to the gas mixture
N	northern/upper boundary of the control volume
N_2	pertinent to nitrogen
o	bottom surface of insulation material
O_2	pertinent to oxygen
r	pertinent to reaction cell
ref	reference condition
S	southern/lower boundary of the control volume
total	pertinent to sum flow
t	top surface
w	pertinent to insulation material
∞	pertinent to environment

Smoldering combustion is of high complexity due to the large number of thermo-chemical and physical sub-processes involved (as outlined by Ohlemiller [8]). Many properties and parameters have to be determined or estimated for proper modeling. It would be very helpful to determine the parameters that have the most significant influence on smoldering (i.e. on conversion time, smoldering front velocity, and temperature of the smoldering front). This is the subject of this study. The results of this work will tell future experimental investigators which physical parameters are crucial for an accurate description of the process and which are, thus, most important to be determined accurately by experimentalists.

Materials investigated in smoldering combustion include: wood [1,2,23], sawdust [2,5], cigarette tobacco [4,17,19,28], cellulose fabric [2,4], flexible foam [4,11,14,26], agro-residues [2,7], dust or forest duff [4,21,24]. Smoldering of these fuels comprises of the heterogeneous sub-processes: drying, pyrolysis and oxidative degradation, char oxidation. Kinetics of the processes show that reaction rates of drying, pyrolysis or oxidative degradation are significantly faster than that of char oxidation [28–30]. What's more, drying and pyrolysis often occur earlier than char oxidation in downward smoldering process. The reason is that oxygen is absolutely necessary for char oxidation, while it is not for drying and pyrolysis. That means when heat is transferred to the adjacent area of fuel bed, drying and pyrolysis occur. But only after oxygen reaches the fuel surface, char oxidation can begin. After pyrolysis the charred fuels are much more similar to each other than the virgin fuels. Due to these, smoldering of char can be regarded as a representative process for most smoldering experiments in context with temperature, smoldering velocity and time. Thus, the theoretical investigations in this study will be conducted with char as a model fuel. The qualitative results of this study should be applicable to any kind of fuel due to the reasons mentioned above.

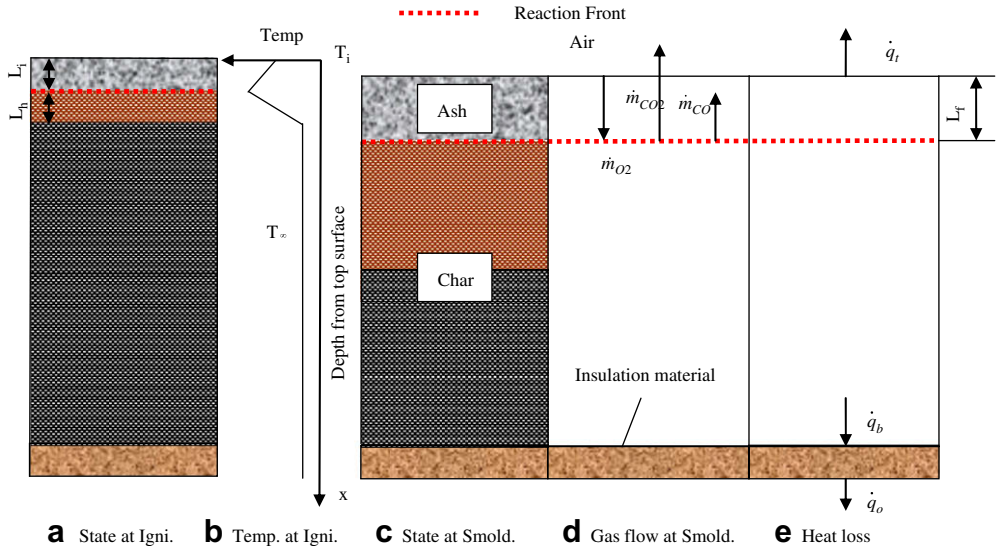

Fig. 1 – Schematic of 1D downward smoldering of char. a) State at ignition. b) Temperature at ignition. c) State at smoldering. d) Gas flow at smoldering. e) Heat loss.

2. Simplified physical model

A schematic of the process is shown in Fig. 1. It is assumed that the porous bed of char only contains carbon and ash. Smoldering propagates downward. There is an infinitesimally thin smoldering front where the carbon gets oxidized. No reaction is taking place outside the reaction front. Above this front, carbon is completely consumed and only the porous ash is left. Below the front there is the char bed. The propagation velocity is very slow (less than mm min^{-1}) and the process is assumed to be quasi-steady, meaning that no gas is accumulated in the finite volumes. Intra-particle temperature gradients are neglected. Solid and fluid phase are assumed to be in thermal equilibrium.

The state of the fuel bed at ignition is illustrated in Fig. 1a and the initial temperature field (representing ignition) is illustrated in Fig. 1b. In a thin ash layer (height L_i) above the smoldering front the temperature increases linearly from the top of the bed ($T = (T_i + T_\infty)/2$) to the smoldering front ($T_f = T_i$). In a thin char layer (height L_h) below the smoldering front the temperature decreases linearly from T_i to T_∞. The rest of the char bed has the initial temperature T_∞.

In the course of smoldering the reaction front propagates downward (Fig. 1c). This is accompanied by shrinkage. The ash layer thickness increases. Mass transfer of gaseous species occurs only above the smoldering front (Fig. 1d). There is total mass flux in upward direction due to the fact that more CO and CO_2 are generated than O_2 consumed. However, both oxygen and nitrogen diffuse in opposite direction to the total mass flux due to the concentration gradient. The net mass flux of nitrogen vanishes, while the net mass fluxes of CO and CO_2 are directed upward. The opposite is true for oxygen.

Heat loss occurs at the top of the bed by radiative and convective heat transfer to the surroundings. At the bottom of the bed heat is conducted to the insulation material. At the bottom of the insulation material, there is radiative and convective heat transfer to the environment (see Fig. 1e).

It is assumed that smoldering extinguishes at temperatures below 523 K.

The velocity of the smoldering front is,

$$V = -\dot{r}_C/\rho_{c\text{-char}} \tag{1}$$

3. Mathematical model and solution

3.1. Reaction

Equation (2) is considered for global carbon oxidation at smoldering front [28].

$$C + (1 - n/2)O_2 \rightarrow nCO + (1 - n)CO_2 \tag{2}$$

The ratio of the product gases can be calculated from [28]:

$$n/(1 - n) = A_{cc} \exp(E_{cc}/RT_f) \tag{3}$$

In general, global reaction kinetics at the front surface can be written as [31]:

$$\dot{r}_C = -M_c \cdot A \exp(E/RT_f)[C_{O_2}] \tag{4}$$

However, there is no pertinent kinetic data for this global reaction in our temperature range. And according to [32], we assume the process is completely transport limited.

3.2. Mass balances

Due to the quasi-steady state assumption, the gaseous species mass balances in the ash layer ($x < L_f$) read:

$$\frac{\partial \dot{m}_i}{\partial x} = 0 \quad \text{with } i = CO,\ CO_2,\ N2,\ O_2 \tag{5}$$

At the reaction front the carbon and the net oxygen flux are converted to CO and CO_2. Thus, the following mass balance holds at $x = L_f$:

$$\dot{r}_C + \dot{m}_{O_2} + \dot{m}_{CO} + \dot{m}_{CO_2} = 0 \tag{6}$$

The net oxygen flux comprises of diffusion (towards the reaction front) and entrained flow with total flow (away from the reaction front) through the ash bed, i.e.:

$$\dot{m}_{O_2} = -\rho_g D_{ash} \frac{\partial w_{O_2}}{\partial x} + w_{O_2} \dot{m}_{total} \tag{7}$$

The total gaseous mass flux density is negative (upward) and given by:

$$\dot{m}_{total} = \dot{m}_{CO} + \dot{m}_{CO_2} + \dot{m}_{O_2} \tag{8}$$

Combining Eq. (7) with (6) and (8), respectively, gives:

$$\dot{m}_{O_2} = -\rho_g D_{ash} \frac{\partial w_{O_2}}{\partial x} - w_{O_2} \dot{r}_C \tag{9}$$

Rearranging Eq. (9) yields:

$$dw_{O_2} / \left[(\dot{m}_{O_2} / \dot{r}_C) + w_{O_2} \right] = -\dot{r}_C / \left(\rho_g D_{ash} \right) \cdot dx \tag{10}$$

The ratio of consumed oxygen to consumed carbon is given by the reaction stoichiometry:

$$\dot{m}_{O_2} / \dot{r}_C = (1 - n/2) \cdot M_{O_2} / M_C \equiv C_1 \tag{11}$$

Assuming that $\dot{r}_C / (\rho_g D_{ash})$ does not depend on x, Eq. (10) can be readily integrated. The oxygen mass fraction at the reaction front can then be determined by:

$$w_{O_2,f} = (C_1 + w_{O_2,\infty}) \exp\left[-\dot{r}_C L_f / (\rho D) \right] - C_1 \tag{12}$$

Due to the assumption of transport limitation, oxygen mass fraction is zero at the reaction front. And then,

$$\dot{r}_C = -\rho_g D_{ash} / L_f \cdot \ln(1 + w_{O_2,\infty} / C_1) \tag{13}$$

3.3. *Energy balances*

3.3.1. *Ash bed, char bed and insulation material*

In the ash layer energy is transported by convection, diffusion, conduction, and radiation. The latter two phenomena are lumped by means of the effective heat conductivity of the bed. Energy transport by diffusion can be neglected. Therefore, the energy balance of a finite volume cell (as shown in Fig. 2) in the ash bed reads:

$$\Delta x_{ash} \rho_{ash} c_a \frac{\partial T}{\partial t} = (\dot{m}_{CO} c_{CO} + \dot{m}_{CO_2} c_{CO_2} + \dot{m}_{O_2} c_{O_2})(T_N - T_S) - \left(k_{eff,ash} \frac{\partial T}{\partial x} \right)_N + \left(k_{eff,ash} \frac{\partial T}{\partial x} \right)_S \tag{14}$$

In the char as well as in the insulation cells no convection occurs. Thus, the energy balances are:

$$\Delta x_c (\rho_{a\text{-}char} c_a + \rho_{c\text{-}char} c_c) \frac{\partial T}{\partial t} = -\left(k_{eff,char} \frac{\partial T}{\partial x} \right)_N + \left(k_{eff,char} \frac{\partial T}{\partial x} \right)_S \tag{15}$$

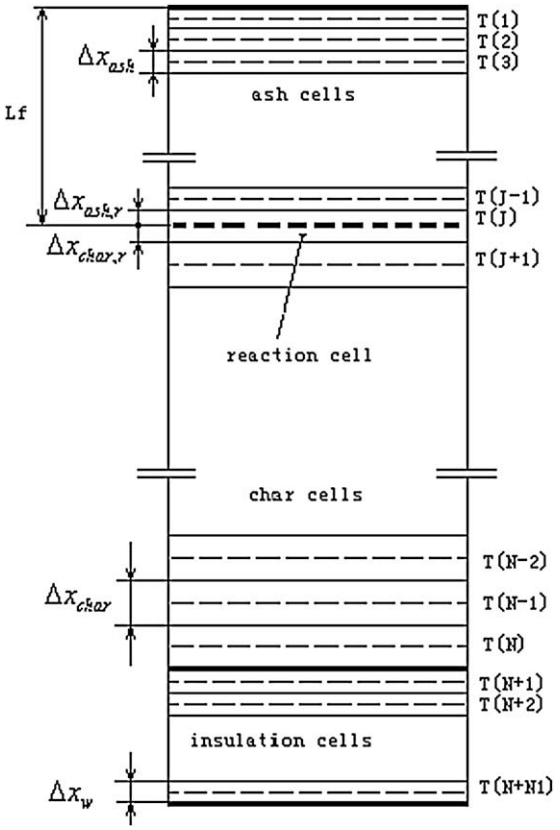

Fig. 2 – Cells for analysis and calculation.

$$\Delta x_w \rho_w c_w \frac{\partial T}{\partial t} = -\left(k_w \frac{\partial T}{\partial x}\right)_N + \left(k_w \frac{\partial T}{\partial x}\right)_S \quad (16)$$

3.3.2. Reaction cell

In the energy balance of the reaction cell it has to be considered that there are two different bed materials present: char below the front and ash above the front. Convection is occurring only across the upper boundary (N = north) while heat conduction and radiation occurs across both boundaries. The heat capacity of the gases is negligible compared to the heat capacities of the solid materials. Hence, the energy balance is derived to be Eq. (17).

$$\begin{aligned}&\left\{\Delta x_{ash,r}\rho_{ash}c_a + \Delta x_{char,r}\left[\rho_{c\text{-}char}c_c + \rho_{a\text{-}char}c_a\right]\right\}\frac{\partial T}{\partial t}\\ &= \dot{r}_C \Delta H^{ref} + \dot{r}_C c_c (T_f - T_{ref}) + \left(\dot{m}_{CO}c_{CO} + \dot{m}_{CO_2}c_{CO_2} + \dot{m}_{O_2}c_{O_2}\right)\\ &\times (T_N - T_{ref}) - \left(k_{eff,ash}\frac{\partial T}{\partial x}\right)_N + \left(k_{eff,char}\frac{\partial T}{\partial x}\right)_S\end{aligned} \quad (17)$$

3.4. Initial and boundary condition

Initial: According to the description in section 1, temperature in the bed at the beginning is,

$$\begin{aligned}&t = 0,\\ &0 < x < L_i, \quad T_0(x) = (T_i + T_\infty)/2 + (T_i - T_\infty)/2 \cdot x/L_i\\ &L_i < x < L_i + L_h, \quad T_0(x) = T_i - (T_i - T_\infty)\cdot(x - L_i)/L_h\\ &x > L_i + L_h, \quad T_0(x) = T_\infty\end{aligned} \quad (18)$$

Boundary: heat loss at the top surface of ash bed is,

$$x = 0, \quad \dot{q}_t = \frac{Nu_t \cdot k_g}{L_c}(T_t - T_\infty) + \varepsilon_a \sigma\left(T_t^4 - T_\infty^4\right) \quad (19)$$

And heat loss at the bottom surface of insulation material is,

$$x = L + L_w, \quad \dot{q}_o = \frac{Nu_o \cdot k_g}{L_c}(T_o - T_\infty) + \varepsilon_w \sigma\left(T_o^4 - T_\infty^4\right) \quad (20)$$

3.5. Void fractions

For ash and char bed, the void fractions are the following:

$$\phi_{ash} = 1 - \rho_{ash}/\rho_a \quad \phi_{char} = 1 - \rho_{c\text{-}char}/\rho_c - \rho_{a\text{-}char}/\rho_a \quad (21)$$

3.6. Transport coefficients

The effective heat conductivities of the two beds are determined according to refs. [20,28],

$$\begin{aligned}&k_{eff,ash} = (1 - \phi_{ash})k_a + \phi_{ash}k_g + 4\phi_{ash}\chi_{ash}\varepsilon_{ash}\sigma T^3;\\ &k_{eff,char} = (1 - \phi_{char})k_{ch} + \phi_{char}k_g + 4\phi_{char}\chi_{char}\varepsilon_{char}\sigma T^3\end{aligned} \quad (22)$$

The oxygen diffusion coefficient can be calculated by [18,28]:

$$D_{ash} = 0.677 D_g \phi_{ash}^{1.18}[T/273]^{1.75} \quad (23)$$

The convective heat transfer coefficients at the top surface of the bed and at out surface of the insulation material were calculated as follows [33]:

$$\begin{aligned}&Nu_t = 0.15\left[Gr\cdot Pr\cdot f_2(Pr)\right]^{1/3} \quad f_2(Pr) = \left[1 + (0.332/Pr)^{\frac{11}{20}}\right]^{-\frac{20}{11}}\\ &Nu_o = 0.6\left[Gr\cdot Pr\cdot f_1(Pr)\right]^{1/5} \quad f_1(Pr) = \left[1 + (0.492/Pr)^{\frac{9}{16}}\right]^{-\frac{16}{9}}\end{aligned} \quad (24)$$

For the top surface, the heat transfer coefficient should be corrected by the Stefan-correction factor [34]:

$$\begin{aligned}C_2 = &\left[\left(\dot{m}_{CO}c_{CO} + \dot{m}_{CO_2}c_{CO_2}\right.\right.\\ &\left.\left. + \dot{m}_{O_2}c_{O_2}\right)/\alpha_t\right]/\left[e^{\left(\dot{m}_{CO}c_{CO} + \dot{m}_{CO_2}c_{CO_2} + \dot{m}_{O_2}c_{O_2}\right)/\alpha_t} - 1\right]\end{aligned} \quad (25)$$

Parameters involved in the equations are summarized in Table 1.

3.7. Numerical solution technique

The finite volume approach is applied in this work. There are four types of finite volumes: ash cells, a reaction cell, char and insulation cells as shown in Fig. 2 (solid rectangles refer to cells). Once the reaction front reaches a char cell, it turns into the reaction cell. After the reaction front has left the cell, it turns into an ash cell. Only the reaction cell is changing its size with time. The shrinkage of the reaction cell can be

Table 1 – Parameters involved in the model.

Property	Value	Source	Property	Value	Source
A_{cc} (s^{-1})	1.0	[28]	k_w (W m^{-1} K^{-1})	0.3	[37],e
c_a (J kg^{-1} K^{-1})	840	[36]	L_w (m)	0.06	[2,7]
c_c (J kg^{-1} K^{-1})	710	[35]	M_g (kg mol^{-1})	30.0	[38],d
c_{CO} (kJ $kmol^{-1}$ K^{-1})	31.5	[38],b	p (Pa)	1.013×10^5	[38]
c_{CO_2} (kJ $kmol^{-1}$ K^{-1})	50.0	[38],b	$w_{O_2,\infty}$	0.233	[38]
c_{O_2} (kJ $kmol^{-1}$ K^{-1})	33.2	[37],e	ε_{ash}	0.9	[37],a
c_w (kJ kg^{-1} K^{-1})	0.9	[28]	ε_{char}	0.9	[37],a
D_g (m^2 s^{-1})	2.0×10^{-5}	[28]	ε_w	0.9	[37],a
E_{cc} (J mol^{-1})	836	[28]	ρ_a (kg m^{-3})	400.0	This work
k_a (W m^{-1} K^{-1})	0.27	[28]	ρ_c (kg m^{-3})	700.0	This work
k_{ch} (W m^{-1} K^{-1})	0.27	[28]	ρ_w (kg m^{-3})	700	[37],e
k_g (W m^{-1} K^{-1})	0.05	[38],c			

a Estimated according to emissivity of non-metallic materials.
b Average value between 500 and 1000 K.
c Average value of air between 500 and 1000 K.
d Estimated according to mole weight of CO, CO_2, N_2, O_2.
e Properties of low density of insulation brick.

Table 2 – Properties of material bed.

	Agro-stalks downward smoldering [7]	Mixed sawdust upward smoldering [2]
Density of biomass bed (kg m^{-3})	40, 50, 60	200
Carbon content in biomass	25%[a]	25%[a]
Density of carbon in char bed, $\rho_{c\text{-}char}$ (kg m^{-3})	**10.0, 12.5, 15.0**	**50.0**
Ash content of biomass	6%[a]	2.5%[a]
Density of ash in char bed, $\rho_{a\text{-}char}$ (kg m^{-3})	**2.4, 3.0, 3.6**	**5.0**
Shrinkage of bed, *sh*	**0.40**[a]	**0.50**[a]
Density of ash in ash bed, ρ_{ash} (kg m^{-3})	**6.0, 7.5, 9.0**	**10.0**
Average void size of ash bed, χ_{ash} (m)	**0.002**	**0.001**
Average void size of char bed, χ_{char} (m)	**0.002**	**0.001**
Original height of fuel bed (m)	**0.5**	**0.1, 0.2, 0.3, 0.4, 0.5, 0.6, 0.9**
Width of fuel bed (m)	**0.4**	**0.3, 0.6, 0.9**

a Estimated according to [39–42].

determined from Eq. (26) and according to Fig. 2. Ash, char, and insulation cells do not change their size.

$$\Delta x_{ash} = sh \times \Delta x_{char} \quad (26)$$

A semi-implicit Euler scheme was used to integrate the system of differential equations. It was implemented in a C-program code. Convergence of the program was tested. Calculation of the typical case showed that the temperature deviation between the total number of 420 cells and 840 cells at the time step of 1 s is less than 0.3 K. And temperature deviation between the time step of 1 s and 0.5 s is less than 0.5 K. Thus total cells of 420 and time step of 1 s was used for calculation. A simulation run on a Pentium 4 processor took approximately 5 min.

4. Results and discussion

4.1. *Qualitative comparison to experimental data*

In order to assess the reliability of the model, two natural smoldering experiments [2,7] were chosen for comparison. Experiments in Ref. [2] were upward smoldering of mixed sawdust in boxes (size 30 cm × 30 cm, 60 cm × 60 cm, 90 cm × 90 cm). The size of fuel is typical and good for future experimental research. Experiments in Ref. [7] were downward smoldering of corn stalks, wheat straw and grass in a stove (height 0.52 m, length 0.55 m, width 0.40 m). Smoldering always extinguished near the bottom (5–10 cm) and the wall (2–3 cm) of stove. And during corn stalk or wheat straw smoldering, flame came out because of the large size of the fuel. However these are the only data we can access for natural vertical smoldering. It should be noted that there are no experimental data for natural downward smoldering of char available in the literature. The properties of the beds are listed in Table 2.

4.1.1. *Smoldering time*

Smoldering time is defined as time interval from ignition until the front temperature is below 523 K. It is a very important parameter when considering fire spread potential and utilization of char smoldering (how long it can heat the space). And this is also an important experimental result. A comparison between experiments of [7] and numerical simulation results of this study is depicted in Fig. 3a. The agreement between simulation and experiment is much better for grass than for wheat straw or corn stalk. That is most probably due to the fact that in the latter two experiments a transition from smoldering to flaming occurred leading to a significantly lower smoldering time. The qualitative trend of increasing smoldering time with increasing bulk density of the bed is reproduced by the model.

The smoldering times reported in [2] refer to upward (reverse) smoldering. It propagates much faster than downward smoldering. The most possible reason might be that carbon is consumed incompletely in upward smoldering. In this case, when char far away above the reaction front was heated more than 523 K or higher, it will react with oxygen around it. The temperature in the spot will be increased and the reaction will be enhanced. If oxygen is completely consumed here, carbon below it will be left unconsumed. Therefore the overestimation of the smoldering time by the model shown in Fig. 3b is consistent. Also the trend of nonlinear increase of smoldering time with initial bed height is reproduced by the model.

4.1.2. *Propagation velocity and temperature at smoldering front*

Predictions referring to the smoldering fronts of the two experiments are shown in Fig. 4. These figures as well as the following are plotted with logarithmic scale in time. Fig. 4a shows that the smoldering front extinguishes for both cases at a height of approximately 8 cm. This is in accordance with the observations in [7]. From Fig. 4b it can be observed that – according to the model – the temperature of the reaction front initially increases at a rate of more than 3 K min^{-1} but after the first hour the temperature decreases slowly. The calculated peak temperatures of the front of agro-stalks and mixed sawdust are 1027 and 1097 K, respectively. They are a little higher than those reported in the literature [2,7,8]. This may be due to neglecting pyrolysis and drying which are endothermic processes. The calculated velocities of the smoldering front (Fig. 4c) are somewhat lower than the ones reported in previous works [2,8] (~10 mm min^{-1}). But that is consistent

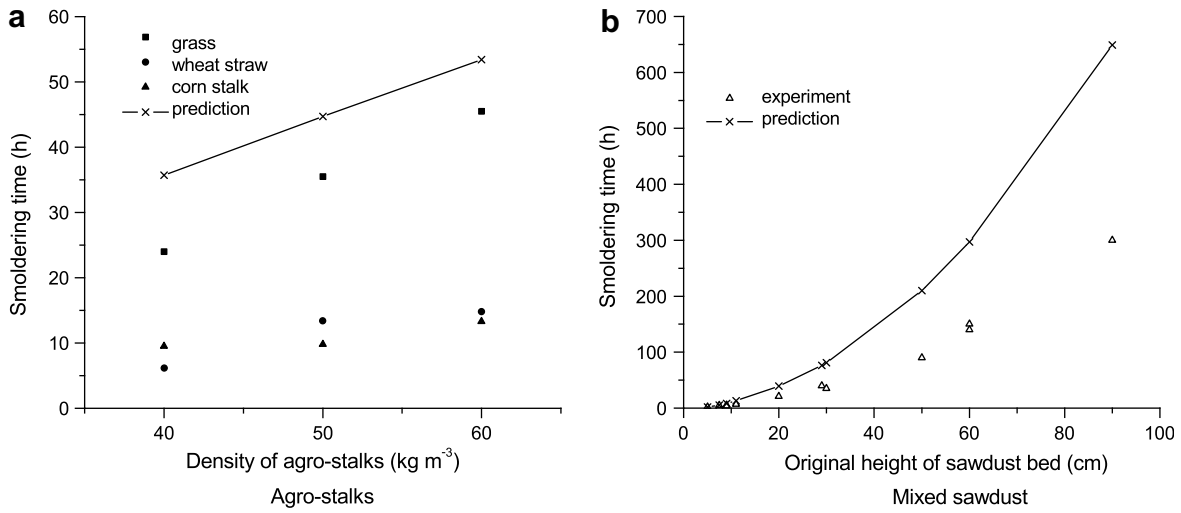

Fig. 3 – Comparison between experimental and simulation results. a) Agro-stalks. b) Mixed sawdust.

since in those works forced or natural reverse smoldering was investigated. These processes are faster than natural forward (i.e. downward here) smoldering.

4.1.3. *Temperature inside the whole bed*

In Fig. 5 the transient temperature development at different positions in the bed is depicted for the two experimental set-ups. It can be observed that during most of the smoldering time the whole inside bed is at elevated temperature, not only the region near the smoldering front. This is consistent with experimental findings of [7]. With this characteristic, oxidative polymer degradation (which is dominated by temperature) in biomass smoldering under the same condition will complete much faster than char oxidation (which is dominated by oxygen content).

The comparisons presented in this subsection indicate that the model predictions are consistent with experimental findings. Therefore, the model is adequate to extract general trends of the process. In the next subsection the influence of several physical parameters will be investigated.

4.2. *Effects of operational condition and fuel properties*

In order to examine the impact of physical properties on the smoldering behavior, a bed of char from sawdust (parameters in Tables 1 and 2) will be considered because this material is widely available for experimentalists around the world. Under these conditions the smoldering front would extinguish before the fuel in the bed is completely consumed.

4.2.1. *Environment*

The influence of the ambient temperature and thickness of bottom insulation material are predicted. Results can be seen in electronics annex 1 in the online version of this article.

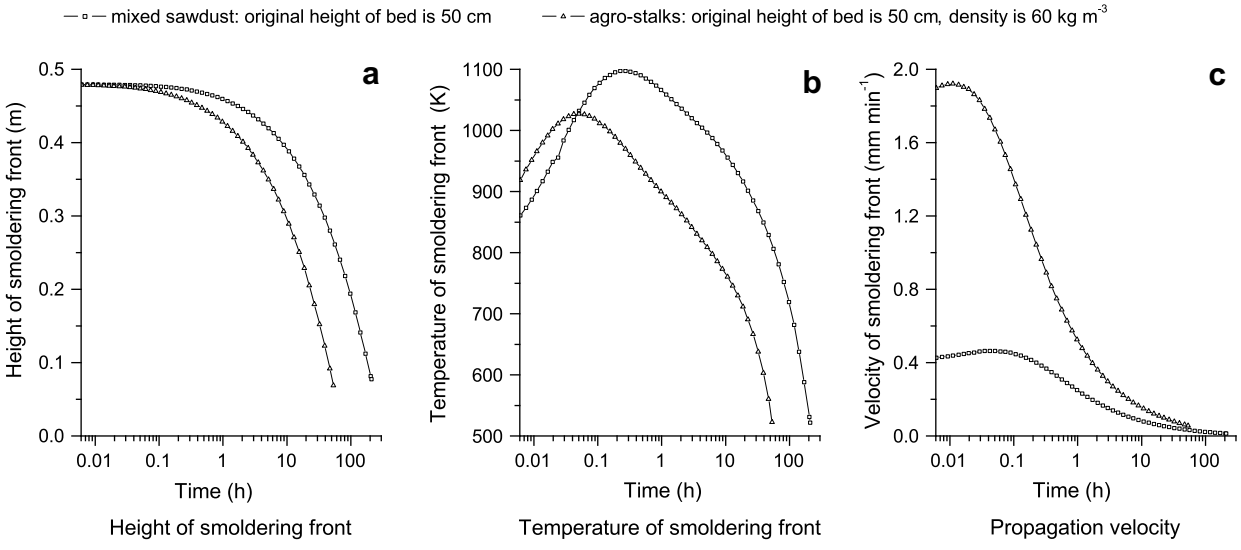

Fig. 4 – Smoldering front characteristics. a) Height of smoldering front. b) Temperature of smoldering front. c) Propagation velocity.

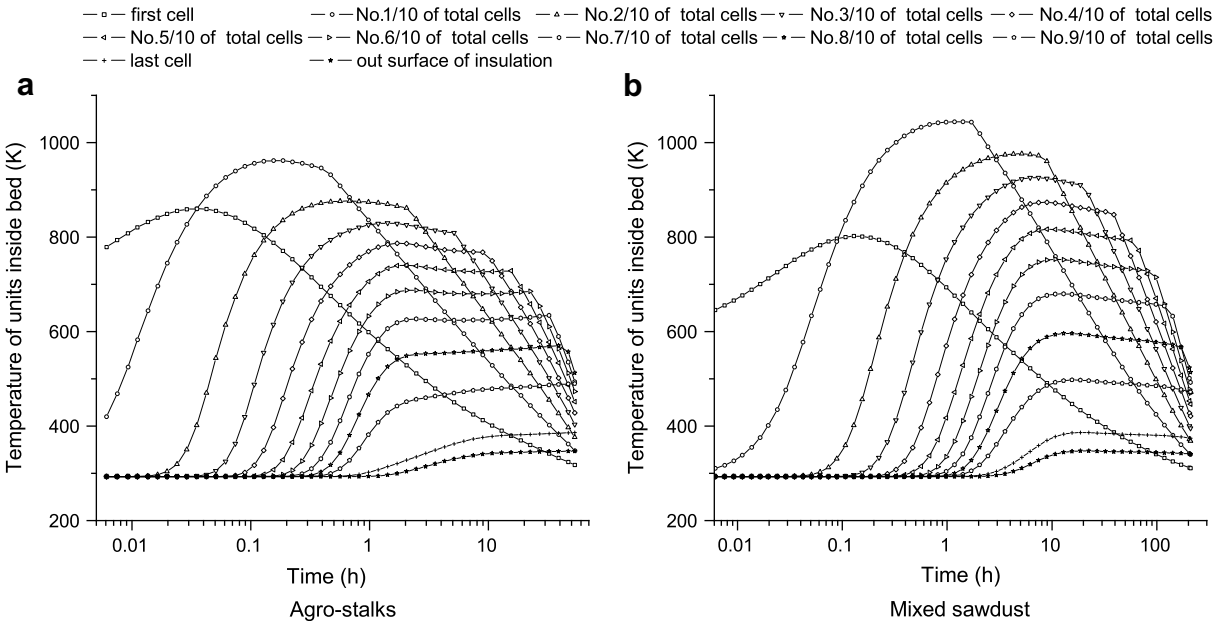

Fig. 5 – Temperature inside the whole fuel bed. a) Agro-stalks. b) Mixed sawdust.

Ambient temperature range is chosen to be 273–313 K according to natural condition. In this range the front velocity is almost unaffected by temperature. An increase of the ambient temperature leads to a slight increase in smoldering time (here 202, 209, 216 h for 273, 293, 313 K) due to less heat loss.

Thickness of insulation materials changes from 5 to 6 cm for experimental set-up to limitless for residue heap [3]. Calculation showed this thickness mainly affects the last stage of smoldering. The thicker the insulation material, the longer the smoldering time is. In case of 6 and 20 cm, increasing the insulation layer thickness has greater impact than increasing the ambient temperature (209 and 240 h for 6 and 20 cm, respectively). That's why smoldering can hold on for a very long time in large volume piled materials. The front velocity is basically unaffected by this thickness.

4.2.2. *Ignition*

In our calculation, initial conditions are assumed. To assess this assumption, effects of ignition temperature and position are calculated. Results can be seen in electronics annex 2 in the online version of this article.

According to the calculation results, the smoldering process is almost unaffected by the ignition temperature. Minor effects of ignition temperature in the range between 673 and 873 K to reaction front temperature are confined to a few minutes after ignition. However, the peak front temperature and the propagation velocity are affected by the ignition

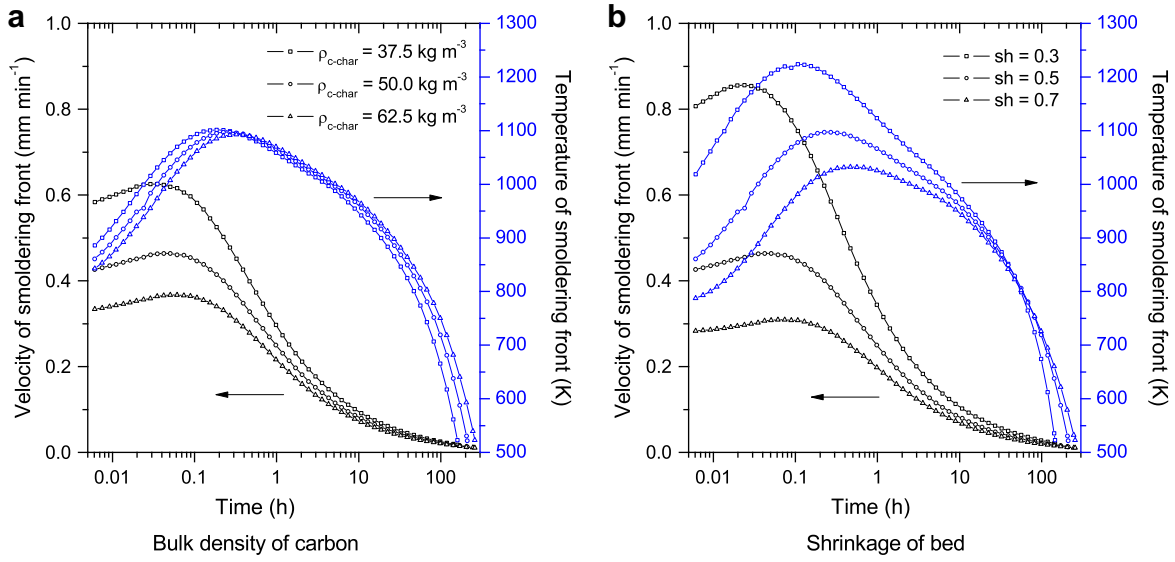

Fig. 6 – Effect of bulk carbon density and shrinkage of bed. a) Bulk density of carbon. b) Shrinkage of bed.

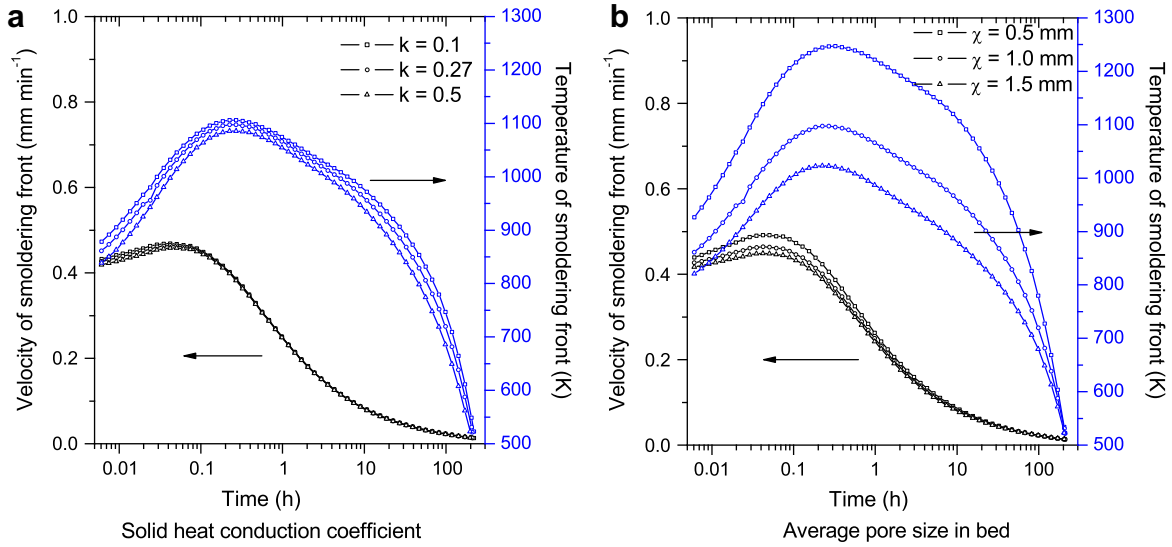

Fig. 7 – Effect of heat transfer. a) Solid heat conduction coefficient. b) Average pore size in bed.

position significantly. The closer to the surface the ignition position, the higher are the peak front temperature and propagation velocity. But 10 h after ignition, the effects are negligible. The smoldering time is almost not affected by the initial conditions.

4.2.3. *Bulk density and shrinkage of char bed*

Smoldering propagation velocity was expressed by the velocity of smoldering front in most literatures [2,8,25,26]. As Palmer observed, differences in bulk density change the velocity of the smoldering front significantly. In order to check this effect, cases of different carbon bulk densities are also calculated. Bulk density of carbon is chosen to be 37.5–62.5 kg m^{-3} because bulk density of most sawdust ranges from 150 to 250 kg m^{-3} and carbon content of sawdust is about 25%. The calculation results in Fig. 6a show that the bulk density in this range does not change temperature inside the smoldering bed significantly (maximum difference was less than 25 K). But the velocity of the smoldering front and the smoldering time (158, 209, 255 h) are affected significantly. However, carbon consumption rate ($\dot{\rho}_{\text{c-char}} \cdot \upsilon$) is almost unaffected by the bulk density in this range. The reason is that the process is transport limited, so it is controlled by void fraction. The void fraction of the ash bed (between 98.27 and 98.96% here) is almost not affected by the change of bulk density in this range.

In our model, oxygen diffuses from top ash surface to reaction front. Thickness of ash bed (decided by the shrinkage of bed) above smoldering front is very important. There were some data on shrinkage of wood particle [37], but data on shrinkage of bed is few. We assess it to be 0.3–0.7 according to our experience in agro-stalks smoldering [7]. Calculation shows (in Fig. 6b) the effect of shrinkage on either temperature or propagation velocity is remarkable. The remarkable effects

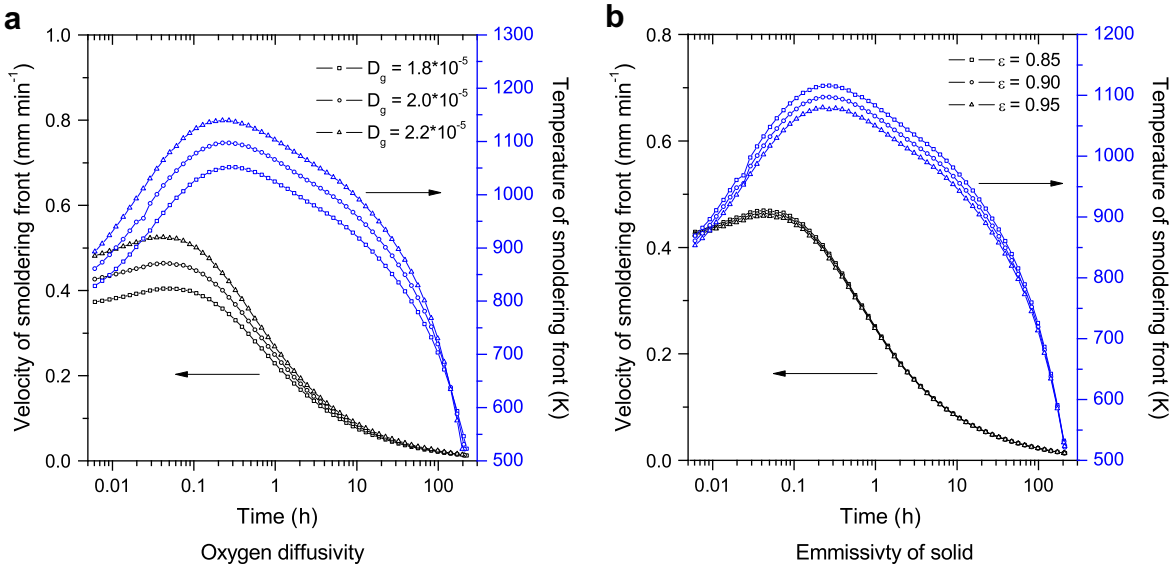

Fig. 8 – Effect of mass transfer and emissivity of solid. a) Oxygen diffusivity. b) Emissivity of solid.

of this parameter make it necessary to measure it accurately in future experiments. Smoldering time (145, 209, 255 h for three cases) is also affected by shrinkage significantly.

4.2.4. *Heat transfer in fuel bed*

The heat conductivity of biomass or char varies according to composition and structure of material. Values between 0.1 and 0.5 W m^{-1} K^{-1} have been reported. Fig. 7a shows that the solid heat conductivity affects the front temperature slightly. The smoldering time is also affected slightly (219, 209, 196 h for 0.1, 0.27 and 0.5 W m^{-1} K^{-1}, respectively). The propagation velocity is not affected. At the last stage of smoldering, the reaction front is deep in fuel bed. Oxygen diffused into the reaction front is very little and the propagation velocity of smoldering is always almost zero so it is not affected by the heat conductivity. However smoldering time is affected by the heat conductivity: If the heat loss is high, this front temperature will decrease to less than 523 K quickly. If the heat loss is low because of low heat conductivity of the fuel bed, the front temperature will keep higher than 523 K for a long time.

According to [17,19], heat transfer by radiation mainly depends on the average void size in the bed. There are few data on this for sawdust char. 0.5–1.5 mm is chosen here for calculation and result was shown in Fig. 7b. It can be concluded that radiation affects front temperature significantly (more than 200 K). Similar to heat conduction, propagation velocity is unaffected. For smoldering time, the smaller the pore size, the longer the smoldering will survive. That is why smoldering often occurs in powder or cellulose materials.

4.2.5. *Mass diffusivity and emissivity of solid*

It is not easy to determine the oxygen diffusivity accurately in gases (N_2, O_2, CO_2, CO) in a porous bed. We also calculate the effect of this property in the range of 1.8×10^{-5}–2.2×10^{-5} m^2 s^{-1} at normal condition and the results are shown in Fig. 8a. It shows that the velocity of smoldering front is proportional to oxygen diffusivity. The temperature of smoldering front is affected considerably (maximum difference is 97 K). And smoldering time was affected slightly. Because of this oxygen diffusivity should be determined accurately in future work.

Emissivity of solid only affects temperature of smoldering front considerably as shown in Fig. 8b. The front velocity is only affected at the beginning very slightly.

4.2.6. *Heat capacity of carbon and ash*

The heat capacity of biomass or char also varies according to composition and structure of material. Effects of heat capacity between 610 and 910 J kg^{-1} K^{-1} are calculated and the result is shown in electronics annex 3 in the online version of this article. It shows that effects of these parameters are negligible.

5. Summary

This theoretical analysis was intended chiefly to serve as guidance for corresponding experimental design. A model for natural downward smoldering in piles of solid fuels was established. Comparing results of numerical simulations with experimental observations showed that the model is adequate to extract general trend of the process. Sensitivity analysis of different physical properties of the bed material with respect to smoldering time, smoldering front velocity and front temperature suggests that in future experiments special attention should be devoted to accurate determination of shrinkage, bulk carbon density, mean void size, and effective oxygen diffusivity in fuel bed.

Acknowledgement

F. He gratefully acknowledges financial support from DAAD (K.C. Wong Fellowship). The authors wish to thank Dr. Michael Oevermann for helpful discussions.

Appendix. Supplementary data

Supplementary data associated with this article can be found, in the online version, at doi:10.1016/j.biombioe.2009.02.008.

REFERENCES

[1] Carvalho ER, Gurgel Veras CA, Carvalho Jr JA. Experimental investigation of smouldering in biomass. Biomass and Bioenergy 2002;22:283–94.
[2] Palmer KN. Smouldering combustion in dusts and fibrous materials. Combustion and Flame 1957;1:129–54.
[3] Nichol D, Tovey NP. Remediation and monitoring of a burning coal refuse bank affecting the Southsea Looproad at Brymbo, North Wales. Engineering Geology 1998;50:309–18.
[4] Ohlemiller TJ. Smoldering combustion. In: DiNenno PJ, Drysdale D, Beyler CL, Walton WD, editors. Handbook of fire protection engineering. 3rd ed. SFPE; 2002. p. 200–10 [chapter 9, Section 2].
[5] Sun WC, Guo XP, Xie MZ, Liu BM. Propagation and gas components of vertical smoldering with natural convection. Journal of Combustion Science and Technology (China) 2002;8:188–91.
[6] Sun WC, Xie M. Energy utilization and characteristic of smoldering pit. Energy of China 1994;8:38–41.
[7] He F, Yi WM, Zha JW, Li YJ. Experiments on smoldering of compressed agro-stalks in natural convection fixed-bed stove. Biomass for energy and industry: 15th European conference & technology exhibition. In: Proceedings of the international conference, Berlin, Germany; 8–11 May 2007. p. 1646–52.
[8] Ohlemiller TJ. Modeling of smoldering combustion propagation. Progress in Energy and Combustion Science 1985;11:277–319.
[9] Ohlemiller TJ, Shaub WM. Products of wood smolder and their relation to wood-burning stoves. Technical report. NBSIR-88-3767. United States; 1988 May 01.
[10] Ohlemiller TJ. Smoldering combustion propagation on solid wood. In: Proceedings of the third international symposium for fire safety science. Scotland, UK; 8–12 July 1991. p. 565–74.
[11] Schult DA, Matkowsky BJ, Volpert VA, Fernandez-Pello AC. Forced forward smolder combustion. Combustion and Flame 1996;104:1–26.

[12] Walther DC, Fernandez-Pello AC, Urban DL. Space shuttle based microgravity smoldering combustion experiment. Combustion and Flame 1999;116:398–414.
[13] Tse SD, Anthenien R, Fernandez-Pello AC. An application of ultrasonic tomographic imaging to study smoldering combustion. Combustion and Flame 1999;116:120–35.
[14] Allmen EM. Numerical modeling of microgravity smoldering combustion in flexible polyurethane foam. Ph.D. thesis, Berkeley, USA: University of California; Spring 2005.
[15] Rein KG, Fernandez-Pello AC, Urban DL. Computational model of forward and opposed smoldering combustion in microgravity. Proceedings of the Combustion Institute 2007; 31:2677–84.
[16] Putzeys O, Bar-Ilan A, Rein KG, Fernandez-Pello AC, Urban DL. The role of secondary char oxidation in the transmission from smoldering to flaming. Proceedings of the Combustion Institute 2007;31:2669–76.
[17] Rostami A, Murthy J, Hajaligol MR. Modeling of a smoldering cigarette. Journal of Analytical and Applied Pyrolysis 2003;66: 281–301.
[18] Rostami A, Murthy J, Hajaligol MR. Modeling of smoldering process in a porous biomass fuel rod. Fuel 2004;83:1527–36.
[19] Saidi MS, Hajaligol MR, Mhaisekar A, Rasouli F. Numerical simulation of burning cigarette during puffing. Journal of Analytical and Applied Pyrolysis 2004;72:141–52.
[20] Buckmaster J, Lozinski D. An elementary discussion of forward smoldering. Combustion and Flame 1996;104:300–10.
[21] El-Sayed SA, Abdel-Latif AM. Smoldering combustion of dust layer on hot surface. Journal of Loss Prevention in the Process Industries 2000;13:509–17.
[22] Leach SV, Rein G, Ellzey JL, Ezekoye OA, Torero JL. Kinetic and fuel property effects on forward smoldering combustion. Combustion and Flame 2000;120:346–58.
[23] Bilbao R, Mastral JF, Aldea ME, Ceamanos J, Betran M. Experimental and theoretical study of the ignition and smoldering of wood including convective effects. Combustion and Flame 2001;126:1363–72.
[24] Krause U, Schmidt M. The influence of initial conditions on the propagation of smoldering fires in dust accumulations. Journal of Loss Prevention in the Process Industries 2001;14: 527–32.
[25] Bakhman NN, Kuznetsov GP, Puchkov VM. Effect of airflow direction and velocity on smoldering waves in combustible porous layers. Combustion, Explosion, and Shock Waves 2002;38:518–24.
[26] Wang JH, Chao CYH, Kong WJ. Experimental study and asymptotic analysis of horizontally forced forward smoldering combustion. Combustion and Flame 2003;135: 405–19.
[27] Souza-Costa F, Sandberg D. Mathematical model of a smoldering log. Combustion and Flame 2004;139:227–38.
[28] Saidi MS, Hajaligol MR, Mhaisekar A, Subbiah M. A 3D modeling of static and forward smoldering combustion in a packed bed of materials. Applied Mathematical Modeling 2007;31:1970–96.
[29] Rogers FE, Ohlemiller TJ. Cellulose insulation material I: overall degradation kinetics and reaction heats. Combustion Science and Technology 1980;24:129–37.
[30] Kashiwagi T, Nambu H. Global kinetics constants for thermal oxidation degradation of a cellulose paper. Combustion and Flame 1992;88:345–68.
[31] Laurendeau NM. Heterogeneous kinetics of coal char gasification and combustion. Progress in Energy and Combustion Science 1978;4:221–70.
[32] Perkins G, Sahajwalla V. Modeling of heat and mass transport phenomena and chemical reaction in underground coal gasification. Chemical Engineering Research and Design 2007;85:329–43.
[33] VDI-Gesellschaft Verfahrenstechnik und chemieingenieurwesen. VDI-warmeatlas. Berlin, Heidelberg: Springer Verlag; 2006. p. Fa1–4.
[34] Bird RB, Stewart WE, Lightfoot EN. Transport phenomena. 2nd ed. John Wiley & Sons, Inc; 2000. p. 704–5.
[35] http://www.chemicool.com/elements/carbon.html; Oct 15th, 2007.
[36] Cortez LAB, Gómez EO. A method for exergy analysis of sugarcane bagasse boilers. Brazilian Journal of Chemical Engineering 1998;15:59–65.
[37] Yang SM. Heat transfer. Beijing, China: Publishing House of People's Education; 1980 [in Chinese].
[38] Yan CJ, Fan W. Combustion theory. Xian, China: Publishing House of Northwestern Polytechnical University; 2005. p. 200–2 [in Chinese].
[39] Senelwa K, Sims REH. Fuel characteristics of short rotation forest biomass. Biomass and Bioenergy 1999;17:127–40.
[40] Kumar RR, Kolar AK, Leckner B. Shrinkage characteristics of casuarina wood during devolatilization in a fluidized bed combustor. Biomass and Bioenergy 2006;30:153–65.
[41] Liao CP, Wu CZ, Yan YJ, Huang HT. Chemical elemental characteristics of biomass fuels in China. Biomass and Bioenergy 2004;27:119–30.
[42] Senneca O. Kinetics of pyrolysis, combustion and gasification of three biomass fuel. Fuel Processing Technology 2007;88:87–97.